Synthesis, structural characterisation and solution chemistry of ruthenium(III) triazole-thiadiazine complexes†

Massimiliano Delferro,[a] Luciano Marchiò,*[a] Matteo Tegoni,[a] Saverio Tardito,[b] Renata Franchi-Gazzola[b] and Maurizio Lanfranchi[a]

Received 24th December 2008, Accepted 25th February 2009
First published as an Advance Article on the web 20th March 2009
DOI: 10.1039/b823271g

Two ruthenium(III) complexes structurally similar to the anticancer compound NAMI were prepared: Na[$RuCl_4$(DMSO)(L1)] (**1**) and Na[$RuCl_4$(DMSO)(L2)] (**2**), where L1 and L2 are differently functionalised triazole-thiadiazine ligands. To facilitate the crystallisation of the complex anions, Na^+ was substituted with the [bis(triphenylphosphoranylidene)ammonium] cation (PPN^+), allowing the X-ray characterisation of PPN[$RuCl_4$(DMSO)(L1)]·$2H_2O$ (**1a**·$2H_2O$) and PPN[$RuCl_4$(DMSO)(L2)]·$3H_2O$ (**2a**·$3H_2O$), respectively. The two compounds undergo stepwise hydrolytic processes, as assessed by means of UV-vis and ^{1}H NMR spectroscopy. The first hydrolytic step consists of the replacement of a chloride anion with a water molecule, with a half-life of 50 min (**1**) and 110 min (**2**), while the subsequent hydrolytic steps are more complicated to describe since more than one product is generated at the same time. The redox potential of the Ru(III)/Ru(II) couple (0.31 V for **1** and 0.28 V for **2**) suggests that these complexes can be reduced in the intracellular environment, in agreement with the "activation by reduction" mechanism proposed for NAMI and NAMI-A. **1** and **2** were tested on a human cancer cell line derived from a fibrosarcoma (HT1080), and on non-cancerous primary human fibroblasts (HF), where they showed a modest inhibitory effect.

Introduction

Ruthenium complexes have received considerable attention in the past two decades, since they have proven to be a valid alternative to *cis*-platin as anticancer compounds against specific tumours.[1,2] The imidazole/sulfoxide complexes NAMI and NAMI-A[3] (Scheme 1) are antimetastatic agents whose activity is not associated with a direct cytotoxicity in tumour cells.[4,5] The substitution of Na^+ with the imidazolium ion confers to NAMI-A a greater chemical stability with respect to NAMI. NAMI-A has successfully completed phase I clinical trials.[6] The other family of Ru(III) complexes endowed with anticancer activity is represented by ICR-like complexes,[7,8] where two nitrogen donor ligands are located in the *trans* positions (Scheme 1). In contrast to NAMI-type complexes, these latter compounds are cytotoxic but do not exhibit anti-metastatic activity.[9] In particular, KP1019 is active against colorectal cancer, where it induces apoptosis. KP1019 has recently completed phase I clinical trials for the treatment of colorectal cancer.[10]

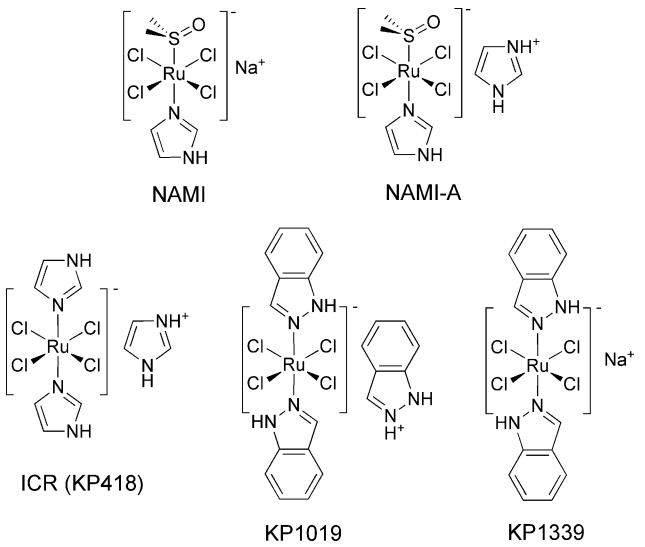

Scheme 1

Despite many efforts dedicated to the mechanism of action of NAMI-A and KP1019, a clear picture of the machinery behind the anticancer properties of these drugs is not yet complete. There are nevertheless some relevant aspects that have been established, where these are related to (i) the redox properties of the Ru(III)/Ru(II) couple and (ii) the hydrolysis of the complexes. Ru(III) species behave as pro-drugs that can be reduced in the hypoxic environment found inside tumour tissue, thus generating labile and more active Ru(II) species that can interact with biomolecules such as DNA.[11,12] This is the so called "activation by reduction" mechanism.[13] In fact, both NAMI-A and KP1019 have

[a]*Dipartimento di Chimica Generale ed Inorganica, Chimica Analitica, Chimica Fisica, Università degli Studi di Parma, Viale G.P. Usberti 17/A, I-43100, Parma, Italy. E-mail: marchio@unipr.it; Fax: +39 0521 905424; Tel: +39 0521 905424*

[b]*Dipartimento di Medicina Sperimentale, Sezione di Patologia Generale e Clinica, Università degli Studi di Parma, Via Volturno 39, I-43100, Parma, Italy*

† Electronic supplementary information (ESI) available: Experimental and calculated FAR-IR spectrum of **1**; ESI-MS spectra of **1** and **2**; ^{1}H NMR spectra of **1** and **2** in D_2O (time range 0–180 min); solvolysis of **1** and **2** in buffered water (pH 7.4); solvolysis of **1** in DMSO; cyclic voltammogram of **2**; antiproliferative activity of **1** and **2** on HF and HT1080 cells. CCDC reference numbers 713340 and 713341. For ESI and crystallographic data in CIF or other electronic format see DOI: 10.1039/b823271g

redox potentials that allow for the reduction of the metal center in a biological environment.[3,14] In parallel with this, the other process that characterises these Ru(III) complexes is the stepwise hydrolysis of chloride ions and, in the case of NAMI-A, also of DMSO.[15,16] This is an important aspect since it appears that the loss of chloro ligands is a requisite for the biological activity of this type of complex. The hydrolysis is even more favoured when Ru(III) has been converted to the more labile Ru(II).

The mechanism through which the Ru(III) complexes are transported once dissolved in biological fluids has also been extensively investigated, and it was shown that proteins such as albumin and transferrin are responsible for the transport of ruthenium species to their site of action.[17–19]

Furthermore, the electrochemical and hydrolytic properties of Ru(III) complexes are strongly dependent on the type of donor atoms surrounding the metal center,[13] and this has stimulated the synthesis of a number of Ru(III) complexes that are structurally similar to NAMI-A[14,20–22] or ICR.[8,14,20,23,24]

Herein, we report the synthesis and X-ray structures of two novel NAMI-like Ru(III) complexes, Na[$RuCl_4$(DMSO)(L1/L2)], where L1 and L2 are N-donor triazole-thiadiazine ligands (Schemes 2 and 3). The molecular structures and biological activity of Cu(II) complexes with sulfurated-triazolo ligands was recently reported,[25] and it was concluded that the N,S coordination to Cu(II) of the thione group of one of these ligands enhances the cytotoxic activity of the resulting complex towards cancer cells. By converting this thione function to thioether groups, as in the case of L1 and L2 ligands, the cytotoxic potential severely diminishes but the cell death process is nonetheless triggered. In the present work we wished to evaluate the biological activity of Ru(III) complexes with sulfurated-triazolo ligands that were able to yield complexes structurally similar to NAMI and NAMI-A.

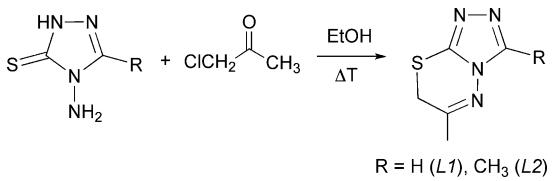

Scheme 2 Ligand synthesis.

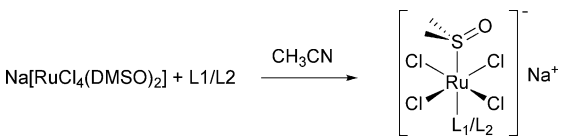

Scheme 3 Synthesis of NAMI-like complexes **1** and **2**.

The hydrolysis and solvolysis of the complexes were investigated by means of UV-vis spectroscopy in non-buffered, buffered (pH 7.4) aqueous solution and in DMSO. In addition, in order to gain information on the electrochemical properties of the complexes, cyclic voltammetry experiments were also performed. The cytotoxic effect of both compounds was studied on normal cells (human fibroblast, HF) and on tumour cells derived from a fibrosarcoma (HT1080).

Results and discussion

Synthesis and characterisation of Na[trans-$RuCl_4$(DMSO)(L1)] (1) and Na[trans-$RuCl_4$(DMSO)(L2)] (2)

The ligands 6-methyl-7*H*-[1,2,4]triazolo[3,4-*b*][1,3,4]thiadiazine (L1) and 3,6-dimethyl-7*H*-[1,2,4]triazolo[3,4-*b*][1,3,4]thiadiazine (L2) can be prepared in high yield in ethanol by reacting chloroacetone with 4-amino-1,4-dihydro-1,2,4-triazole-5-thione or 4-amino-1,4-dihydro-3-methyl-1,2,4-triazole-5-thione, respectively (Scheme 2). The parent ligands can adopt different coordination modes with metal centers, the most common of which is represented by N,S chelation with the thione and amino functions.[26–30] The conversion of the thione group into a thioether induces a dramatic decrease of the coordination capability of the sulfur atom, and the nitrogen atoms of the triazole ring then become the preferred donor sites.[31,25]

The Ru(III) complexes **1** and **2** were prepared starting from the ruthenium precursor Na[$RuCl_4$(DMSO)$_2$], in analogy to the procedure reported in the literature for the synthesis of NAMI[3] (Scheme 3).

The solution characterisation of **1** and **2** was performed by means of ESI-MS spectrometry and ^{1}H NMR spectroscopy. The ESI-MS spectra of **1** and **2** dissolved in acetonitrile show the peaks of the [$RuCl_4$(DMSO)(L1/L2)]$^-$ anionic complexes and the corresponding molecular fragments: [$RuCl_4$(DMSO)]$^-$, [$RuCl_4$(L1/L2)]$^-$, and [$RuCl_4$]$^-$ (see ESI†). The ^{1}H NMR spectra of **1** and **2** in D_2O present several broad peaks, in accordance with the presence of paramagnetic Ru(III) metal ions (Fig. 1). The assignment of the signals of **1** and **2** was performed by comparison with the ^{1}H spectra of similar Ru(III) complexes and by means of the inversion recovery technique, which provides the longitudinal relaxation time T1.[32] In fact, nuclei that are close to Ru(III) will exhibit a shorter T1 if compared with nuclei that are at a certain distance from the paramagnetic center, such as solvent molecules. In the present case, the determination of T1 values is hindered by the overlap of the broad signals, and only the peak at −1 ppm of **2** could be properly analysed. The T1 value of this signal is ~10 ms, considerably smaller than that of the acetone present as an impurity (~200 ms). It is nonetheless evident from the experiment that the remaining broad peaks exhibit comparable T1 values. The broad signal at ~−15 ppm is consistent with S-coordinated DMSO as reported for other NAMI-like complexes.[3,22] A tentative assignment of L1 and L2 signals was performed by considering that their paramagnetic shift depends on their distance from the Ru(III) center: for **1**, 0.9 ppm (–CH_2–), 0.71 ppm (C–H), 0.62 ppm (–CH_3); for **2**, 1.1 ppm (CH_3), 0.8 ppm (–CH_2–), −1 ppm (–$CH_3^{triazole}$).

Any attempt to grow single crystals of **1** and **2** suitable for X-ray structural determination were unsuccessful. Nevertheless, when the Na^+ cation was replaced with PPN^+ [bis(triphenylphosphoranylidene)ammonium], crystals of PPN[$RuCl_4$(DMSO)(L1)]·2H_2O (**1a**·2H_2O) and PPN[$RuCl_4$(DMSO)(L2)]·3H_2O (**2a**·3H_2O) were obtained. The molecular structures of the complex anion of **1a**·2H_2O and **2a**·3H_2O are depicted in Figs. 2 and 3, respectively. Relevant geometric parameters are reported in Table 1.

In both compounds, the metal adopts an octahedral geometry, and the S-coordinated DMSO is in the *trans* position to L1 or L2, and four chloride ions occupy the equatorial positions.

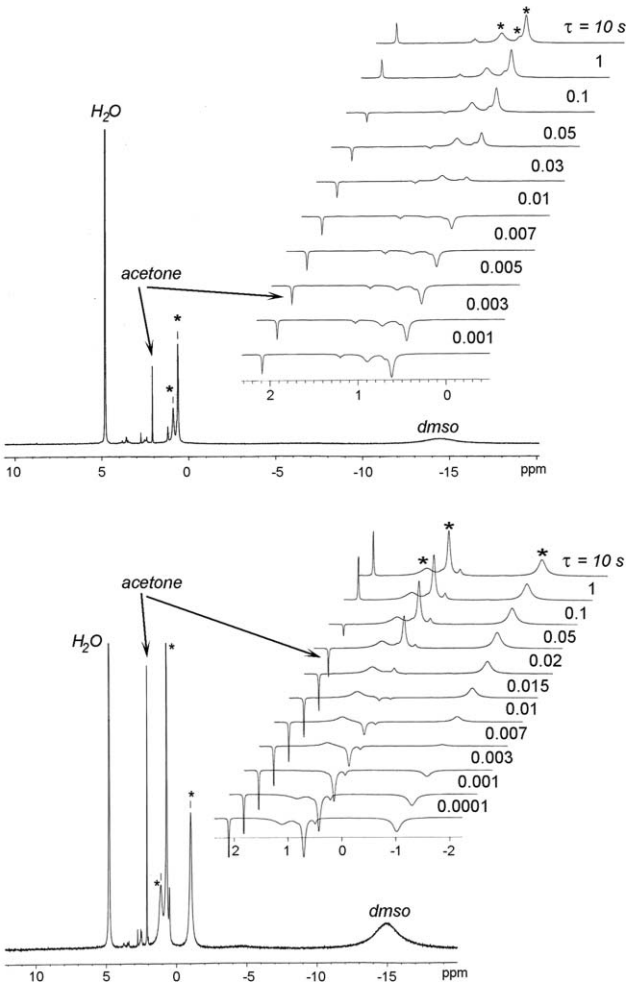

Fig. 1 ^{1}H NMR spectra of **1** (above) and **2** (below) together with the inversion recovery experiments. Asterisks define protons of the ligands L1 and L2.

Table 1 Selected bond lengths [Å] for **1a**·2H$_2$O and **2a**·3H$_2$O

1a·2H$_2$O			
Ru-N(11)	2.079(8)	Ru-Cl(2)	2.372(3)
Ru-S(12)	2.310(3)	Ru-Cl(3)	2.323(3)
Ru-Cl(1)	2.363(3)	Ru-Cl(4)	2.344(3)
P(1)-N(12)	1.582(7)	P(2)-N(12)	1.602(7)
2a·3H$_2$O			
Ru-N(21)	2.134(2)	Ru-Cl(2)	2.3477(9)
Ru-S(12)	2.2981(9)	Ru-Cl(3)	2.3677(9)
Ru-Cl(1)	2.3734(9)	Ru-Cl(4)	2.3700(9)
P(1)-N(12)	1.579(2)	P(2)-N(12)	1.574(2)

Interestingly, L1 and L2 are coordinated to the metal through two different nitrogen atoms of the triazole ring, where this may be attributed to the comparable donor ability of the two nitrogen atoms. The discriminating factor in determining which nitrogen atom participates in the metal coordination may be due to the different steric hindrance that is present close to the N(11) atoms of L1 and L2 and by the perturbation that this would cause on the $RuCl_4$ equatorial plane: a hydrogen atom in L1 favours the

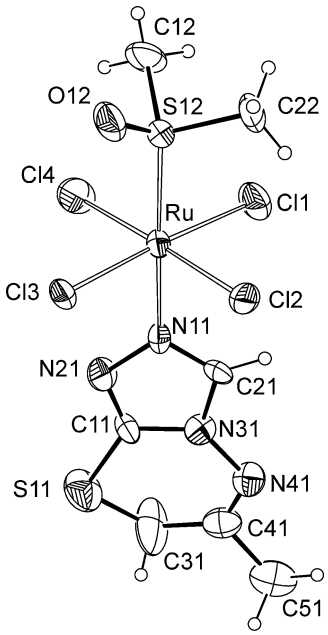

Fig. 2 Ortep drawing of **1a**·2H$_2$O. Thermal ellipsoids are drawn at the 30% probability level. The PPN$^+$ cation and the crystallization water molecules were omitted for clarity.

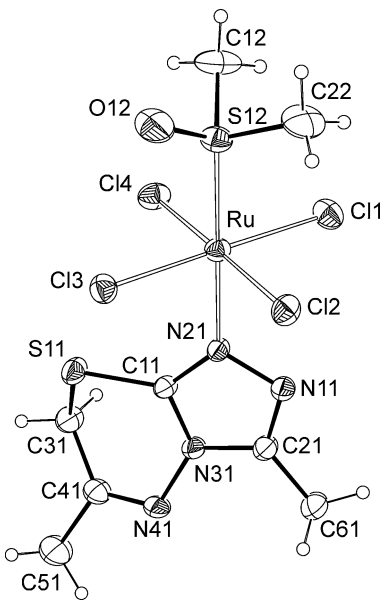

Fig. 3 Ortep drawing of **2a**·3H$_2$O. Thermal ellipsoids are drawn at the 30% probability level. The PPN$^+$ cation and the crystallization water molecules were omitted for clarity.

coordination of N(11) with respect to N(21), whereas for L2, the steric hindrance would not constitute a discriminating factor for the N(11) and N(21) coordination if we assume that the van der Waals radii of a sulfur atom and a methyl group are nearly equivalent. Additional proof that the steric hindrance may play a role in the preferred coordination of the complex derives from the observation that, in both compounds, the molecular plane of the triazole ligand is bisecting the Cl(1)–Ru–Cl(2) angle. In **1a**·2H$_2$O, the O1w water molecule is involved in hydrogen bonds (HBs) with O2w (d[O1w–O2w] = 2.83(1) Å) and with the oxygen atom of a

Table 2 UV-vis data (λ_{max} and ε) for the Ru(III) complexes

	λ_{max} (nm), ε	λ_{max} (nm), ε
Na[$RuCl_4$(L1)(DMSO)]	398, 3690	485, 590
Na[$RuCl_4$(L2)(DMSO)]	398, 3418	485, 600
NAMI	390, 3644	451, 488[a]

[a] ref. 3.

DMSO ligand of an adjacent complex molecule (d[O1w–O(12)'] = 2.881(1) Å; ′ = x, y, $z-1$). In addition, the O2w molecule acts as a HB donor with respect to the sulfur atom of L1 (d[O2w–S(11)] = 3.39(1) Å). In **2a**·3H_2O, the O1w water molecule acts as a HB donor with respect to Cl(1) (d[O1w–Cl(1)] = 3.444(3) Å) and O2w (d[O1w–O2w] = 2.859(5) Å), whereas the O3w water molecule acts as a HB donor with respect to O2w (d[O3w–O2w] = 2.873(5) Å) and N(11) (d[O3w–N(11)] = 2.885(4) Å).

Far-infrared spectra were recorded for **1** and **2** (see ESI†), and the assignment of the Ru–Cl stretching frequencies was made on the basis of FAR-IR spectra of similar compounds.[7,33–37] The L1 and L2 coordination at the metal atom causes a shift to higher values of the Ru–S stretching vibration frequency with respect to the Ru(III) precursor. The new peaks that appear around 450 cm^{-1} can be attributed to the Ru–N stretching.

Solution stability assays (Hydrolysis and solvolysis).

Compounds **1** and **2** are soluble in water, acetonitrile and DMSO, and the UV-vis spectra recorded in water or acetonitrile are characterised by relatively intense bands at ~400 nm, and by a second and weaker band at ~485 nm (Table 2). The former band can be ascribed to $\pi Cl \rightarrow t_{2g}Ru$ LMCT (Ru-Cl) transitions involving the four coplanar chlorides.[38] These findings are in line with the data reported for NAMI or NAMI-like complexes.[3,23]

In order to investigate the hydrolysis and solvolysis processes, **1** and **2** were dissolved in water or DMSO and their UV-vis spectra were recorded over a period of 50 h (water, Fig. 4), 24 h (DMSO, ESI†), or 3 h (buffered water pH = 7.4, ESI†). In water, different families of spectra can be identified for both complexes, indicating at least two/three different consecutive reactions. The first family of spectra can be restricted to the 0–170 min interval (Fig. 4, upper diagram), and it is characterised by a decrease of the band at 398 nm and a clear isosbestic point at 370 nm. After this time, the band at 398 nm tends to decrease, but the isosbestic point at 370 nm is lost and a new broad band appears at 545 nm in spectra up to 50 h (Fig. 4, lower diagram). Although two apparent isosbestic points appeared at 366 and 480 nm in the 540–3000 min time range, a careful evaluation of the spectra through the Evolving Factor Analysis[39,40] revealed that they are not proper isosbestic points and that at least three different species should be present in solution. For all processes, however, the $\pi Cl \rightarrow t_{2g}Ru$ LMCT band centered at 398 nm tends to decrease, suggesting that the reactions occurring at the metal center most likely involve the replacement of chloride ions with water molecules, as observed for other NAMI-A-type complexes.[20,22] Following the hydrolysis with ^1H NMR experiments in the 0–3 h time range, the appearance of the uncoordinated DMSO/ligand signals indicate that the hydrolysis also affects these moieties, albeit to a lesser extent with respect to the chloride hydrolysis. In fact, the signals of the free ligands do not increase significantly with respect to those of the coordinated ones (ESI†). While the process occurring in the 0–170 min time range produce only a small change in the shape of the absorption spectra, it is worth noting that the subsequent reactions produce a marked spectral change, as evidenced by the appearance of the new band at 540 nm. Moreover, the processes that occur in the 540–3000 min interval may involve a more extensive hydrolysis with substitution of the triazole, chloride or DMSO ligands, giving rise to a more complicated spectral set. The spectral behaviour of **2** is analogous to that of **1**, and the spectral changes over a 50 h time course are reported in the ESI.†

The spectra collected for **1** and **2** in the 0–170 min time interval were used to calculate the kinetic rate constant for the first process by means of a least squares regression on all of the 270–700 wavelengths. The spectra could be fitted with a first order kinetic law ($v = k$[complex]) and, for both complexes, the absorbance residuals after the fitting process were less than 1% over the entire spectral range. A plot of the experimental and calculated absorbance at two representative wavelengths (342 and 398 nm) is reported in Fig. 5.

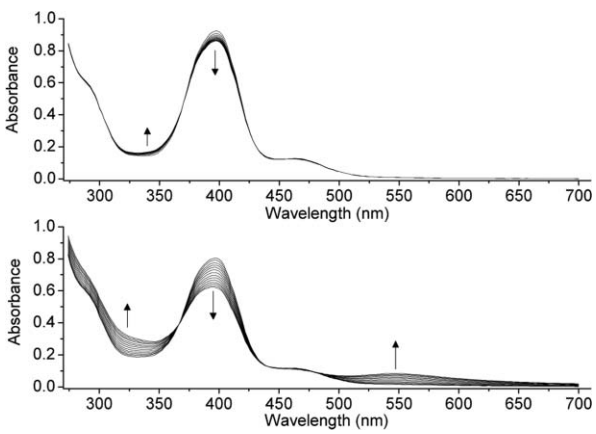

Fig. 4 Upper diagram: UV-vis spectra of **1** Na[$RuCl_4$(DMSO)(L1)] in water at 7.5 min intervals (0–170 min after dissolution). Lower diagram: UV-vis spectra of **1** in water at 180 min intervals (540–3000 min after dissolution).

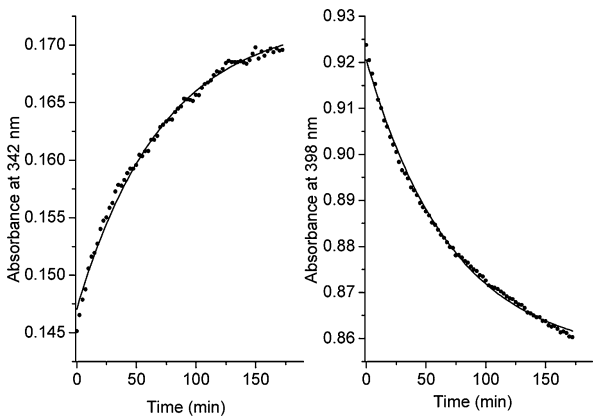

Fig. 5 Experimental (dots) and calculated (lines) absorbances for the hydrolytic reaction of Na[$RuCl_4$(DMSO)(L1)] (**1**) in water (0–170 min after dissolution) at 342 and 398 nm.

Attempts to fit the spectra in the range 170–3000 min with different kinetic models gave inconsistent results, suggesting that several processes may occur at the same time. Although the spectral change for the two complexes is similar, the reaction rate for the first process (0–170 min) for complex **1** is *ca.* twice that of complex **2**. In fact, k is $2.33(7) \times 10^{-4}$ s^{-1} for **1**, and $1.05(7) \times 10^{-4}$ s^{-1} for **2**, corresponding to a half-life of 50 and 110 min, respectively. These rate constants are within the same order of magnitude as expected by assuming the same hydrolytic process for both complexes, and their difference can be ascribed to the different coordination behaviour of L1 *vs.* L2 to the metal center. These rate constants are one order of magnitude higher than those determined for NAMI-A in acidic buffers.[41] On the other hand, when the hydrolysis is measured in buffered water solution at physiological pH (7.4), the first hydrolysis process is much faster, having an half-life of approximately 9 min (ESI†). This is in agreement with the values determined for the NAMI-A-like complexes with substituted triazolo-pyrimidine[22] and thiazole[20] ligands in buffered solutions (pH 7.4). The hydrolysis profile of **1** and **2** at pH 7.4 is characterized in the first step by the decrease of the bands centered at 395, and 465 nm, and by the increase of the band centered at 350 nm. In a second stage, this latter band decreases, and additional bands centered at 330, 440 and 575 nm prevail.

The solvolysis in DMSO was investigated due to the fact that in some cases, this solvent is employed for cytotoxic studies at a concentration of 9‰ in water. The spectrophotometric profiles of **1** and **2** as a function of time are reported in the ESI.† After 2 h, the band at 410 nm shifts to 421 nm and the spectrum becomes superimposable with that of the precursor [*trans*-$RuCl_4(DMSO)_2]^-$. This may imply that L1 and L2 in **1** and **2**, respectively, are replaced by DMSO molecules within a few hours. This is probably a consequence of the *trans*-effect exerted by the DMSO molecules of the complexes.[42]

Electrochemistry

The redox behaviour of NAMI-A was extensively investigated,[43] and the formal redox potential $E°'$ measured in different aqueous solutions varied in the range of +0.268/+0.254 V. These values have important consequences for the biological properties of the compound. In fact, they imply that the Ru(III) → Ru(II) reduction is possible in the intracellular environment of proliferating cells. This is due to the high concentration of glutathione in the cytosol and to the hypoxic environment present in tumour tissues.[44] Following the reduction, NAMI-A first undergoes hydrolysis of the imidazole ligand and, in a second stage, a chloride ion is substituted by a water molecule.[43]

The redox behaviour of **1** and **2** is very similar to that of NAMI-A. In Fig. 6, the cyclic voltammogram of **1** in non-buffered water is shown. In the first scan, a reduction peak is observed at 0.27 V (peak A), which is associated with the oxidation peak at 0.36 V (peak B). After the reduction, some of the Ru(II) complex undergoes hydrolysis and gives rise to an additional oxidation peak in the reverse scan at 0.51 V (peak C), which is then associated with a new reduction peak at 0.42 V (peak D). The $[RuCl_4(DMSO)(L1)]^-/[RuCl_4(DMSO)(L1)]^{2-}$ redox couple that defines the A–B system exhibits a redox potential of 0.31 V *vs* NHE, in line with NAMI-A-type complexes

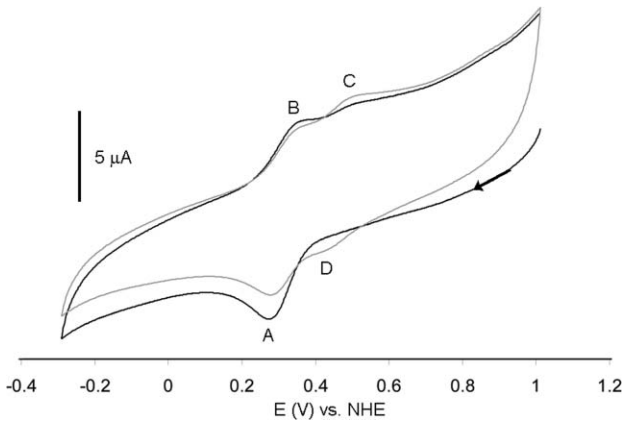

Fig. 6 Cyclic voltammograms of a 5×10^{-4} M solution of **1** dissolved in water. Supporting electrolyte: KNO_3 0.1 M. Scan rate: 10 mV/s. First scan (black line), second scan (gray line).

containing nitrogen donor ligands.[17] The redox behaviour of **2** is analogous to that of **1**, with the redox potential for the $[RuCl_4(DMSO)(L2)]^-/[RuCl_4(DMSO)(L2)]^{2-}$ couple being 0.28 V. The cyclic voltammogram of **2** recorded at 25 mV/s is reported in the ESI.†

Antiproliferative studies

Complexes **1** and **2** were tested on the human cancer cell line derived from a fibrosarcoma (HT1080), and on non-cancerous primary human fibroblasts (HF) in order to evaluate their effect on cell proliferation. The compounds tested show a modest inhibitory effect on the viability of both cell types (ESI†). At the highest concentration tested (100 μM), all complexes cause a ≈20% and 10% decrease in the viability in HT1080 and HF, respectively, when compared to untreated cells. This effect is possibly due to a decrease in the proliferation rate of both normal and cancer cells, since no signs of cytotoxicity were evident in treated cell cultures.

It is known that NAMI-A exerts its antitumour effects by reducing the metastatic potential of cancer cells.[45] Its mechanism of action is related to the ability to decrease the motility of cells, impairing their invasiveness. For this reason, its antimetastatic activity is not generally associated with an antiproliferative/cytotoxic effect. Thus far, we cannot exclude the effectiveness of these new Ru complexes as antimetastatic agents, and more focused biological studies are needed to prove this hypothesis.

Conclusions

Ru(III) complexes are actively investigated as valid alternatives to *cis*-platin as anticancer compounds.[1] The most promising ruthenium compounds are represented by NAMI-A and KP1019, which have recently completed phase I clinical trials.[6,10] The mechanism of action of NAMI and NAMI-A has been partly interpreted, and it involves Ru(III) → Ru(II) reduction in the intracellular environment followed by partial hydrolysis of the complex. Prompted by these results, a number of Ru(III) compounds have been prepared by modifying the nitrogen donor ligand, with the aim of improving the biological properties and the therapeutic potential of the resulting complexes. In the present work, two Ru(III) complexes, which are structurally similar to NAMI, were prepared and

structurally characterised, namely Na[*trans*-$RuCl_4$(DMSO)(L1)] (**1**) and Na[*trans*-$RuCl_4$(DMSO)(L2)] (**2**), where L1 and L2 are triazole-thiadiazine ligands. The two complexes behave similarly to NAMI-A once dissolved in water, as they are subjected first to the hydrolysis of a chloride ion, and in later stages to a more extensive aquation. Furthermore, the redox potential of the Ru(III)/Ru(II) couple (0.31 and 0.28 V for **1** and **2**, respectively) would imply the reduction of the two complexes in the hypoxic environment of tumour tissues.[13] In order to evaluate the antitumour properties of the two complexes, preliminary antiproliferative studies were performed with normal cells (HF) and tumour cells derived from a fibrosarcoma (HT1080). Both complexes showed only modest antiproliferative activity against HT1080 cells (20%), and more studies are necessary in order to investigate their antimetastatic potential.

Experimental

General procedures

All solvents and reagents are commercially available and were used as received, except Na[$RuCl_4$(DMSO)$_2$],[34] 4-amino-1,4-dihydro-1,2,4-triazole-5-thione[29] and 4-amino-1,4-dihydro-3-methyl-1,2,4-triazole-5-thione,[46] which were prepared as described elsewhere. Elemental analyses were carried out by Carlo Erba mod. EA1108 microanalyser. Infrared spectra were recorded on a Nicolet 5PC FT-IR spectrometer in KBr pellets (4000–400 cm^{-1}) and in CsI pellets (600–200 cm^{-1}). Electrospray ionization mass spectrometry (ESI-MS) was carried out in acetonitrile with a Micromass ZMD instrument (conc. = 2×10^{-4} M for all complexes); the given m/z values, originating from the most intense isotope, were obtained by the mass linearization procedure. Expected and experimental isotope distributions were compared in order to assign molecular fragment peaks. ^{1}H NMR spectra were recorded on a Bruker Avance 300 spectrometer, and chemical shifts are reported in ppm referenced to residual solvent protons (DMSO-d_6 and D_2O). The paramagnetic Ru(III) complexes **1** and **2** were characterised in D_2O using the inversion recovery pulse technique: π–τ–π/2-FID. 10 spectra were recorded with τ that varied in the range of 0.00001–10 sec. Cyclic voltammetry was performed using an Autolab PGSTAT 20 potentiostat (Ecochemie, The Nethrlands) with GPES 4.9 software in a one-compartment three-electrode cell using a 3.0-mm diameter platinum disk working electrode, a platinum rod counter electrode and Ag/AgCl/KCl (3M) as a reference electrode ($E°$ = +211.5 mV at 20 °C). Cyclic voltammograms were collected in nonbuffered water solution using KNO_3 as the supporting electrolyte. The voltammograms were referenced to NHE.

2*H*-3-methyl-[1,2,4]-triazole-[3,4-*b*]-[1,3,4]-thiadiazine (L1). To a suspension of 4-amino-1,4-dihydro-1,2,4-triazole-5-thione (2.734 g, 23.5 mmol) in absolute ethanol (30 mL) was added chloroacetone (95%) (2 mL, 23.5 mmol) with stirring. The brown clear solution was refluxed for 4 h. The mixture was cooled to room temperature and neutralised with sodium bicarbonate and vacuum dried. The solid was then treated with absolute ethanol and ethyl acetate (1:1), and the inorganic salts ($NaHCO_3$, NaCl) were removed by filtration. The volatiles were removed *in vacuo*. The brown sticky product was triturated with hexane, which gave a brown precipitate (Yield: 91%). $C_5H_6N_4S$ (154.19): calcd. C, 38.95; S, 20.80; H, 3.92; N, 36.34; found: C, 38.62; S, 20.72; H, 3.89; N, 36.29. ^{1}H NMR (DMSO-d_6): δ = 8.97 (s, 1H, CH), 3.87 (s, 2 H, CH_2), 2.26 (s, 3 H, CH_3) ppm. IR (KBr, cm^{-1}): 3112 m, 3096 m, 2956 m, 2902 w, 1629 m, 1488 s, 1426 s, 1281 s, 1160 s, 1021 m, 948 s, 795 s, 641 s.

2*H*-3,6-dimethyl-[1,2,4]-triazole-[3,4-*b*]-[1,3,4]-thiadiazine (L2). To a suspension of 4-amino-1,4-dihydro-3-methyl-1,2,4-triazole-5-thione (2.095 g, 16 mmol) in absolute ethanol (30 ml) was added chloroacetone (95%) (1.35 ml, 16 mmol) with stirring. The yellow clear solution was refluxed for 4 h. The mixture was cooled to room temperature and neutralised with sodium bicarbonate and vacuum dried. The solid was then treated with absolute ethanol and ethyl acetate (1:1), and the inorganic salts ($NaHCO_3$, NaCl) were removed by filtration. The clear brown solution was concentrated, and upon addition of diethyl ether, a brown precipitate formed (Yield: 89%). $C_6H_8N_4S$ (%): calcd C, 42.84; S, 19.06; H, 4.79; N, 33.31; found: C, 42.70; S, 18.99; H, 4.72; N, 33.26. ^{1}H NMR (DMSO-d_6): δ = 3.80 (s, 2H, CH_2), 2.37 (s, 3H, $CH_3^{triazole}$), 2.28 (s, 3H, $CH_3^{thiadiazine}$) ppm. IR (KBr, cm^{-1}): 2991 w, 2962 m, 2900 m, 1540 s, 1471 s, 1441 s, 1394 s, 1296 m, 1017 m, 808 m.

Na[*trans*-$RuCl_4$(DMSO)(L1)] (1). An orange solution of Na[*trans*-$RuCl_4$(DMSO)$_2$] (0.180 g, 0.43 mmol) in CH_3CN (10 mL) was added to a solution of **L1** (0.098 g, 0.64 mmol) in CH_3CN (5 mL). The mixture was stirred overnight. A brown precipitate formed, which was filtered, washed with an ethanol/diethyl ether mixture (1:1), dried in a vacuum and collected (Yield: 78%). $C_7H_{12}Cl_4N_4ONaRuS_2$ (498.20): calcd. C, 16.87; H, 2.42; N, 11.24; S, 12.87; found: C, 16.75; H, 2.38; N, 11.20; S, 12.81. ^{1}H NMR: (D_2O): δ = 0.89 (broad), 0.71 (broad), 0.62 (broad), -14.52 (broad, DMSO) ppm. IR (KBr cm^{-1}): 3114 m, 3005 w, 2919 w, 2896 w, 1635 w, 1505 s, 1459 s, 1419 m, 1384 w, 1312 w, 1096 s, 1021 s, 971 w, 784 m. Far-IR (CsI cm^{-1}): 458, 436, 364, 343. ESI-MS (CH_3CN, negative ion mode): m/z = 475.7 [$RuCl_4$(DMSO)(L1)]$^-$, 395.8 [$RuCl_4$(L1)]$^-$, 321.8 [$RuCl_4$(DMSO)]$^-$, 243.6 [$RuCl_4$]$^-$.

PPN[*trans*-$RuCl_4$(DMSO)(L1)]·$2H_2O$ (1a·$2H_2O$). **1** (0.050 g, 0.010 mmol) was dissolved in water (2 mL). To the orange solution, bis(triphenylphosphoranylidene)ammonium chloride (PPN^+Cl^-) (0.057 g, 0.01 mmol) dissolved in 1 ml of water/ethanol (1:0.2 v:v) was added with stirring. Light-orange crystals of PPN[*trans*-$RuCl_4$(DMSO)(L1)]·$2H_2O$ (**1a**·$2H_2O$) suitable for X-ray analysis formed immediately (Yield: 73%).

Na[*trans*-$RuCl_4$(DMSO)(L2)] (2). An orange solution of Na[*trans*-$RuCl_4$(DMSO)$_2$] (0.180 g, 0.43 mmol) in CH_3CN (10 mL) was added to a solution of L2 (0.107 g, 0.64 mmol) in CH_3CN (5 mL). The mixture was stirred overnight. A brown-orange precipitate formed, which was filtered, washed with ethanol/diethyl ether, and dried *in vacuo*. (Yield: 68%). $C_8H_{14}Cl_4N_4NaORuS_2$ (512.23): calcd. C, 18.75; H, 2.75; N, 10.93; S, 12.52. Found: C, 18.62; H, 2,71; N, 10.90; S, 12,45. ^{1}H NMR (D_2O): δ = 1.10 (broad), 0.71 (broad), -1.0 (broad), -14.5 (broad, DMSO) ppm. IR (KBr, cm^{-1}): 3018 w, 2964 w, 2925 w, 1558 m, 1471 m, 1428 m, 1308 m, 1292 m, 1095 s, 1025 s, 685 w. Far-IR (CsI, cm^{-1}): 448, 431, 356, 332. ESI-MS (CH_3CN, negative ion mode): m/z = 491.9 [$RuCl_4$(DMSO)(L2)]$^-$, 404.9 [$RuCl_4$(L2)]$^-$, 321.8 [$RuCl_4$(DMSO)]$^-$, 243.6 [$RuCl_4$]$^-$.

Table 3 Crystallographic data of **1a**·2H_2O and **2a**·3H_2O

	1a·2H_2O	**2a**·3H_2O
Formula	$C_{43}H_{46}Cl_4N_5O_3P_2RuS_2$	$C_{44}H_{50}Cl_4N_5O_4P_2RuS_2$
Fw	1049.78	1081.82
cryst. syst.	Monoclinic	Monoclinic
Space group	*Cc*	$P2_1/c$
a,Å	10.277(4)	11.063(2)
b,Å	31.887(9)	14.691(3)
c,Å	14.738(7)	30.977(6)
α	90	90
β	104.333(9)	99.83(2)
γ	90	90
V,Å^3	4679(3)	4961(2)
Z	4	4
D/Mgm^{-3}	1.490	1.449
λ	Mo Kα (0.71073 Å)	Mo Kα (0.71073 Å)
T/K	293(2)	293(2)
μ, mm^{-1}	0.765	0.726
Rflc collected/unique	24350/8320	53967/11291
R_{int}	0.1118	0.0730
No. of params. refined	545	581
GOF	0.688	1.036
R_1(obs.), wR_2	0.0459, 0.0560	0.0431, 0.0582
Lrgst diff. peak/hole Å^{-3}	0.480 and -0.375	0.730 and -0.464

$R_1 = \sum\|F_o\| - |F_c\|/\sum|F_o|$; $wR_2 = [\sum w(F_o^2 - F_c^2)^2/\sum wF_o^4]^{\frac{1}{2}}$

PPN[*trans*-$RuCl_4$(DMSO)(L2)]·3H_2O (2a·3H_2O). Na[*trans*-$RuCl_4$(DMSO)(L2)] (0.05 g, 0.0097 mmol) was dissolved in water (2 mL). To the orange solution, bis(triphenylphosphoranylidene)ammonium chloride (PPN^+Cl^-) (0.056 g, 0.0097 mmol), dissolved in 1 ml water/ethanol (1:0.2 v:v), was added with stirring. Yellow crystals of PPN[*trans*-$RuCl_4$(DMSO)(L2)]·3H_2O (**2a**·3H_2O) suitable for X-ray analysis were immediately obtained (Yield: 70%).

Crystallographic structure determination

A summary of data collection and structure refinement for PPN[$RuCl_4$(DMSO)(L1)]·2H_2O (**1a**·2H_2O) and PPN[$RuCl_4$-(DMSO)(L2)]·3H_2O (**2a**·3H_2O) are reported in Table 3. Single crystal data were collected with a Bruker AXS Smart 1000 area detector diffractometer (Mo Kα; α = 0.71073 Å). Cell parameters were refined from the observed setting angles and detector positions of selected strong reflections. Intensities were integrated from several series of exposure frames covering a hemisphere of reciprocal space.[47] No crystal decay was observed. Absorption correction using the program SADABS[48] was applied, which resulted in minimum and maximum transmission factors of 0.974–1.000 (**1a**·2H_2O) and 0.755–1.000 (**2a**·3H_2O). The structures were solved by direct methods (SIR97)[49] and refined with full-matrix least squares (SHELXL-97)[50] using the Wingx software package.[51] Non-hydrogen atoms were refined anisotropically. The hydrogen atoms of the two water molecules of **1a**·2H_2O could not be located from the difference Fourier map, whereas the hydrogen atoms of the three water molecules of **2a**·3H_2O were found and refined. The remaining hydrogen atoms were placed at their calculated positions. The maximum and minimum peaks on the final difference Fourier maps corresponded to 0.480/–0.375 (**1a**·2H_2O) and 0.730/–0.464 (**2a**·3H_2O) e Å^{-3}. Graphical material was prepared with the ORTEP3 for Windows[51] program.

UV-visible and solution studies

UV-Vis spectra were recorded in the 270–700 nm range on Perkin-Elmer lambda 25 and Varian Cary 50 spectrophotometers using matched, teflon-capped quartz cuvettes (d = 1 cm). Solvolysis of **1** and **2** in water was studied by dissolving the complexes in doubly distilled water ($C_{Ru} = 2.5 \times 10^{-4}$ M) and collecting the spectra over time using dedicated Varian software (every 2.5 for 0–540 min, and every 30 min for 540–3000 min). Solvolysis of **1** and **2** in buffered water solution (HEPES 50 mM, NaCl 0.9%, pH = 7.4) was performed in the 0–300 min time range collecting the spectra every 30 sec. Solvolysis of **1** and **2** in DMSO was studied by dissolving the complexes at $C_{Ru} = 2 \times 10^{-4}$ M and collecting the spectra 1, 3, 6, 8, 24, 32, 48, 72 and 96 h after dissolution. Calculations of the kinetic rate constants for the solvolysis processes in water were performed using the software SPECFIT/32,[40] using the whole spectral range (270–700 nm).

Cell lines and culture conditions

Human fibroblasts (HF) were derived from a skin biopsy from an healthy donor and were stored in liquid nitrogen at a stock of 10^6 cells/ml. HT1080, a cell line originating from a human fibrosarcoma, were provided from the "Instituto Zooprofilattico di Brescia". HT1080 cells and HF were routinely grown in Dulbecco's Modified Eagle's Medium (DMEM) supplemented with 100 U/ml penicillin, 100 µg/ml streptomycin and 10% fetal bovine serum (FBS). Cells were cultured at 37 °C in a 5% CO_2 atmosphere at pH 7.4.

Viability assay

The cells used for this study were in the exponential growth phase. The cells were seeded in 96-well plates at a density of 10000 and 4000 cells/well for HF, and 4000 for HT1080, in 100 µl of medium and incubated for 24 h. The growth medium was then substituted with a fresh one containing the substances to be tested at the experimental concentrations. **1** and **2** were dissolved in 0.9% NaCl physiological solution. 6 wells were treated with vehicle (control) and 6 wells were treated with *cis*-platin (25 µM), which is used as a standard cytotoxic drug. Cell viability was tested after 48 h with the Resazurin assay as previously described:[52] growth medium was replaced with a DMEM solution of resazurin. After 2 h, the samples' fluorescence was measured at 572 nm with a microplate reader (Wallac 1420 Victor^2 Multilab Counter).

Acknowledgements

This work was supported by Università degli Studi di Parma, Italy. We thank CIM (Centro Interdipartimentale Misure "Giuseppe Casnati") of the University of Parma for the use of the NMR facilities. We are also grateful to CIRCMSB (Consorzio Interuniversitario di Ricerca in Chimica dei Metalli nei Sistemi Biologici).

Notes and references

1 M. J. Clarke, F. C. Zhu and D. R. Frasca, *Chem. Rev.*, 1999, **99**, 2511.
2 M. J. Clarke, *Coord. Chem. Rev.*, 2002, **232**, 69.
3 E. Alessio, G. Balducci, A. Lutman, G. Mestroni, M. Calligaris and W. M. Attia, *Inorg. Chim. Acta*, 1993, **203**, 205.

4 G. Sava, S. Pacor, G. Mestroni and E. Alessio, *Clin. Exp. Metastasis*, 1992, **10**, 273.
5 G. Sava, I. Capozzi, K. Clerici, G. Gagliardi, E. Alessio and G. Mestroni, *Clin. Exp. Metastasis*, 1998, **16**, 371.
6 J. M. Rademaker-Lakhai, D. van den Bongard, D. Pluim, J. H. Beijnen and J. H. M. Schellens, *Clin. Cancer Res.*, 2004, **10**, 3717.
7 B. K. Keppler, W. Rupp, U. M. Juhl, H. Endres, R. Niebl and W. Balzer, *Inorg.Chem.*, 1987, **26**, 4366.
8 K. G. Lipponer, E. Vogel and B. K. Keppler, *Met.-Based Drugs*, 1996, **3**, 243.
9 C. G. Hartinger, S. Zorbas-Seifried, M. A. Jakupec, B. Kynast, H. Zorbas and B. K. Keppler, *J. Inorg. Biochem.*, 2006, **100**, 891.
10 C. G. Hartinger, M. A. Jakupec, S. Zorbas-Seifried, M. Groessl, A. Egger, W. Berger, H. Zorbas, P. J. Dyson and B. K. Keppler, *Chem.Biodivers.*, 2008, **5**, 2140.
11 J. Malina, O. Novakova, B. K. Keppler, E. Alessio and V. Brabec, *J. Biol. Inorg. Chem.*, 2001, **6**, 435.
12 D. Pluim, R. C. A. M. van Waardenburg, J. H. Beijnen and J. H. M. Schellens, *Cancer Chemother. Pharmacol.*, 2004, **54**, 71.
13 E. Reisner, V. B. Arion, B. K. Keppler and A. J. L. Pombeiro, *Inorg. Chim. Acta*, 2008, **361**, 1569.
14 E. Reisner, V. B. Arion, M. Fatima, C. G. da Silva, R. Lichtenecker, A. Eichinger, B. K. Keppler, V. Y. Kukushkin and A. J. L. Pombeiro, *Inorg. Chem.*, 2004, **43**, 7083.
15 G. Sava, A. Bergamo, S. Zorzet, B. Gava, C. Casarsa, M. Cocchietto, A. Furlani, V. Scarcia, B. Serli, E. Iengo, E. Alessio and G. Mestroni, *Eur. J. Cancer*, 2002, **38**, 427.
16 A. Kung, T. Pieper, R. Wissiack, E. Rosenberg and B. K. Keppler, *J. Biol. Inorg. Chem.*, 2001, **6**, 292.
17 M. Groessl, E. Reisner, C. G. Hartinger, R. Eichinger, O. Semenova, A. R. Timerbaev, M. A. Jakupec, V. B. Arion and B. K. Keppler, *J. Med. Chem.*, 2007, **50**, 2185.
18 M. Brindell, I. Stawoska, J. Supel, A. Skoczowski, G. Stochel and R. van Eldik, *J. Biol. Inorg. Chem.*, 2008, **13**, 909.
19 L. Messori, P. Orioli, D. Vullo, E. Alessio and E. Iengo, *Eur. J. Biochem.*, 2000, **267**, 1206.
20 P. Mura, M. Camalli, L. Messori, F. Piccioli, P. Zanello and M. Corsini, *Inorg. Chem.*, 2004, **43**, 3863.
21 I. Turel, M. Pecanac, A. Golobic, E. Alessio, B. Serli, A. Bergamo and G. Sava, *J. Inorg. Biochem.*, 2004, **98**, 393.
22 A. H. Velders, A. Bergamo, E. Alessio, E. Zangrando, J. G. Haasnoot, C. Casarsa, M. Cocchietto, S. Zorzet and G. Sava, *J. Med. Chem.*, 2004, **47**, 1110.
23 P. Mura, F. Piccioli, C. Gabbiani, M. Camalli and L. Messori, *Inorg. Chem.*, 2005, **44**, 4897.
24 V. B. Arion, E. Reisner, M. Fremuth, M. A. Jakupec, B. K. Keppler, V. Y. Kukushkin and A. J. L. Pombeiro, *Inorg. Chem.*, 2003, **42**, 6024.
25 S. Tardito, O. Bussolati, M. Maffini, M. Tegoni, M. Giannetto, V. Dall'Asta, R. Franchi-Gazzola, M. Lanfranchi, M. A. Pellinghelli, C. Mucchino, G. Mori and L. Marchiò, *J. Med. Chem.*, 2007, **50**, 1916.
26 F. Dallavalle, F. Gaccioli, R. Franchi-Gazzola, M. Lanfranchi, L. Marchiò, M. A. Pellinghelli and M. Tegoni, *J. Inorg. Biochem.*, 2002, **92**, 95.
27 R. W. Clark, P. J. Squattrito, A. K. Sen and S. N. Dubey, *Inorg. Chim. Acta*, 1999, **293**, 61.
28 R. M. McCarrick, M. J. Eltzroth and P. J. Squattrito, *Inorg. Chim. Acta*, 2000, **311**, 95.
29 T. W. Kajdan, P. J. Squattrito and S. N. Dubey, *Inorg. Chim. Acta*, 2000, **300**, 1082.
30 P. Aslanidis, P. J. Cox, S. Divanidis and P. Karagiannidis, *Inorg. Chim. Acta*, 2004, **357**, 1063.
31 M. B. Cingi, M. Lanfranchi, M. A. Pellinghelli and M. Tegoni, *Eur. J. Inorg. Chem.*, 2000, **4**, 703.
32 H. Gunther, *NMR Spectroscopy*, John Wiley & Sons Ltd, 2001.
33 K. Nakamoto, *Infrared and Raman Spectra of Inorganic and Coordination Compounds*, Part B, 5th ed., John Wiley & Sons, New York, 1997.
34 E. Alessio, G. Balducci, M. Calligaris, G. Costa, W. M. Attia and G. Mestroni, *Inorg. Chem.*, 1991, **30**, 609.
35 A. Garza-Ortiz, P. U. Maheswari, M. Siegler, A. L. Spek and J. Reedijk, *Inorg. Chem.*, 2008, **47**, 6964.
36 B. Serli, E. Zangrando, T. Gianfeffara, L. Yellowlees and E. Alessio, *Coord. Chem. Rev.*, 2003, **245**, 73.
37 M. Zuber and Z. Ciunik, *Polyhedron*, 2007, **26**, 1643.
38 C. M. Duff and G. A. Heath, *J. Chem. Soc. Dalton Trans.*, 1991, **9**, 2401.
39 H. Gampp, M. Maeder, C. J. Meyer and A. D. Zuberbuhler, *Talanta*, 1986, **33**, 943.
40 R. A. Binstead, A. D. Zuberbühler, and B. Jung, SPECFIT/32 ver. 3.0.35, 2004, Spectrum Software Associates, http://www.biologic.info/rapid-kinetics/software.html.
41 M. Bouma, B. Nuijen, M. T. Jansen, G. Sava, A. Flaibani, A. Bult and J. H. Beijnen, *Int. J. Pharm.*, 2002, **248**, 239.
42 S. A. Cotton, *Chemistry of Precious Metals*, Blackie Academic & Professional, London, UK, 1997.
43 M. Ravera, S. Baracco, C. Cassino, P. Zanello and D. Osella, *J. Chem. Soc. Dalton Trans.*, 2004, **15**, 2347.
44 F. Q. Schafer and G. R. Buettner, *Free Rad. Biol. Med.*, 2001, **30**, 1191.
45 F. Frausin, V. Scarcia, M. Cocchietto, A. Furlani, B. Serli, E. Alessio and G. Sava, *J. Pharmacol. Exp. Ther.*, 2005, **313**, 227.
46 M. B. Cingi, F. Bigoli, M. Lanfranchi, M. A. Pellinghelli, A. Vera and E. Buluggiu, *J. Chem. Soc. Dalton Trans.*, 1992, **21**, 3145.
47 *SMART (control) and SAINT (integration) software for CCD systems*, Bruker AXS, Madison, WI, USA, 1994.
48 *Area-Detector Absorption Correction*, Siemens Industrial Automation, Inc., Madison, WI, 1996.
49 A. Altomare, M. C. Burla, M. Camalli, G. L. Cascarano, C. Giacovazzo, A. Guagliardi, A. G. G. Moliterni, G. Polidori and R. Spagna, *J. Appl. Cryst.*, 1999, **32**, 115.
50 G. M. Sheldrick, *SHELX97. Programs for Crystal Structure Analysis (Release 97–2)*. University of Göttingen, Germany, 1997.
51 L. J. Farrugia, *J. Appl. Cryst*, 1999, **32**, 837.
52 S. Tardito, O. Bussolati, F. Gaccioli, R. Gatti, S. Guizzardi, J. Uggeri, L. Marchiò, M. Lanfranchi and R. Franchi-Gazzola, *Histochem. Cell Biol.*, 2006, **126**, 473.